Asphaltene Adsorption onto Self-Assembled Monolayers of Alkyltrichlorosilanes of Varying Chain Length

Salomon Turgman-Cohen,[†] Daniel A. Fischer,[‡] Peter K. Kilpatrick,[†,§] and Jan Genzer*,[†]

Department of Chemical & Biomolecular Engineering, North Carolina State University, Raleigh, North Carolina 27695-7905, and Ceramics Division, National Institute of Standards and Technology, Gaithersburg, Maryland 20899

ABSTRACT The adsorption of asphaltenes onto flat silica surfaces modified with self-assembled monolayers (SAMs) of alkyltrichlorosilanes of varying thickness due to a variable number of carbon atoms (N_C) has been studied by means of contact angle measurements, spectroscopic ellipsometry, and near-edge X-ray absorption fine structure spectroscopy. The extent of asphaltene adsorption was found to depend primarily on the ability of the SAM layer to shield the underlying silicon substrate from interacting with the asphaltenes present in solution. Specifically, asphaltene adsorption decreased with an increase in N_C and/or an increase in SAM grafting density, σ_{SAM}, (i.e., number of SAM molecules per unit area). The effect of the solvent quality on the extent of asphaltene adsorption was gauged by adsorbing asphaltenes from toluene, 1-methylnaphthalene, tetralin, decalin, and toluene−heptanes mixtures. The extent of asphaltene adsorption was found to increase proportionally with a decrease in the Hildebrand solubility parameter of the solvent.

KEYWORDS: asphaltenes • self-assembled monolayers • alkyltrichlorosilanes • NEXAFS • ellipsometry • wettability

INTRODUCTION

Pipeline fouling due to deposition of heavy organics from crude oils represents a significant problem for the petroleum industry because it decreases pipeline flow rates, thus seriously hindering oil refining and production (1). In severe cases, fouling of pipelines requires costly cleaning procedures or even pipeline replacement, often resulting in complete plant shutdown. Asphaltenes, defined broadly as a fraction of crude oil insoluble in a low-boiling paraffinic solvent (*n*-pentane or *n*-heptane) but soluble in aromatic solvents such as toluene or benzene (2), are in many cases responsible for this detrimental pipeline contamination. Asphaltenes represent a chemically and structurally heterogeneous group of organic molecules present in oil; they are typically characterized as macromolecules with high degrees of aromaticity and polarity that possess a propensity to form colloidal aggregates in solution, stabilize water-in-oil emulsions, and have the ability to adsorb onto solid−liquid and liquid−liquid interfaces. Devising ways in which to prevent or substantially lessen the adsorption of asphaltenes onto solid surfaces is therefore be beneficial to the petroleum industry.

Research pertaining to the adsorption of asphaltenes onto solid surfaces has recently experienced an upsurge primarily because of soaring petroleum prices and the possibility that refining crudes with high asphaltenic content can become a viable commercial venture. The adsorption of asphaltenes onto solid substrates has been characterized by means of a wide variety of experimental methods, including contact angle (CA) measurements (3−5), ultraviolet−visible (UV−vis) spectrometry (6), atomic force microscopy (4, 7, 8), photothermal surface deformation (9−12), Fourier transform infrared spectroscopy (8), quartz crystal microbalance (QCM) gravimetry (13−15), X-ray photoelectron spectroscopy (XPS) (6, 16), and ellipsometry (17, 18). The adsorption of asphaltenes onto solid surfaces is governed by the characteristics of the asphaltenic solutions, including the asphaltene source and concentration as well as the solvent quality. Akhlaq et al. (5) investigated the adsorption of asphaltenes onto glass plates by monitoring the variation in the CA of a glycerol droplet on the asphaltene-treated surfaces. The CA of glycerol on the glass plates increased after asphaltene treatment, suggesting that asphaltenes shielded the polar substrate from the probing liquid. Akhlaq and co-workers also monitored the increase in the CA for depositions from solvents of varying polarity, that is, toluene, tetrahydrofuran, chloroform, and *n*-heptane−toluene (Heptol) mixtures. The CA of the plates was reported to increase with a decrease in the solvent polarity. This observation was attributed to higher amounts of asphaltenes adsorbed on the glass surface, which effectively shielded the substrate from the probing droplet. In a latter work, Alboudwarej et al. (19) characterized the adsorption of asphaltenes onto metals by monitoring the asphaltene concentration in solution using UV−vis spectrometry. Adsorption experiments from dilute solutions

© 2009 American Chemical Society

(<0.06% w/w) onto stainless steel, iron, and aluminum powders indicated monolayer adsorption of asphaltenes, suggesting that the adsorption was limited by the number of adsorption sites on the metallic surface. The same authors observed that the amount of asphaltenes adsorbed on the surfaces decreased in the following fashion: stainless steel > iron > aluminum. However, no plausible explanation was offered in the original publications to explain these observations. Alboudwarej and co-workers also noted that asphaltenes dissolved in Heptol mixtures adsorbed to a higher extent relative to adsorption taking place from pure toluene solutions. This observation, consistent with other studies, was reconciled by considering the decrease in the solubility of asphaltenes and the formation of larger supramolecular aggregates in Heptol solutions relative to toluene (20−22).

QCM and optical ellipsometry represent two practical tools applicable in characterizing asphaltene adsorption. QCM monitors the mass of adsorbed asphaltenes in situ from a wide range of solution concentrations (13). Unlike QCM, which is not limited by the transparency of the deposition solution, ellipsometry does not permit in situ measurements. However, ellipsometry can provide information about both the thickness of the adsorbed asphaltenes with subnanometer precision and the average optical properties of the adsorbed layer (23). Ekholm et al. (13) studied the effects of the solution concentration and solvent quality on the adsorption of asphaltenes onto a gold surface. Exposure of the QCM crystal to the asphaltene solutions resulted in rapid shifts in the crystal's oscillating frequency, indicating adsorption of small supramolecular aggregates. The authors observed that adsorption of asphaltenes from toluene solutions increased continuously as a function of increasing concentration, with no plateau observed at high solute concentrations. This behavior was attributed to strong asphaltene−asphaltene interactions in toluene that resulted in the formation of multilayers on the gold substrate. Adsorption of asphaltenes from Heptol mixtures with equimolar compositions was also characterized, and a larger extent of asphaltene adsorption was detected relative to equivalent concentrations of asphaltenes in toluene, emphasizing the effect of the solvent quality on the extent of asphaltene adsorption. Labrador et al. (17) employed null ellipsometry to monitor the adsorption of asphaltenes onto glass surfaces after 24 or 48 h of asphaltene adsorption. Their results supported earlier evidence indicating that strong asphaltene−asphaltene interactions contributed to the formation of thick multilayers.

While most of the research on asphaltene adsorption onto solid surfaces has been carried out on hydrophilic metallic or glass substrates, the effect of modifying these substrates chemically has not been explored systematically. Hannisdal et al. (24) studied the stabilizing power of silica particles on water-in-oil and oil-in-water emulsions. Although the main focus of their study pertained to the stability of emulsions as the wettability of the particles was varied, the authors provided insights into the adsorption of asphaltenes onto chemically modified silica particles. In their work, commercially available neat silica particles and particles modified with [2-(methacryloxy)propyl]trimethoxysilane, poly(dimethylsiloxane), and dimethyldichlorosilane were exposed to asphaltene solutions. The authors established visually that hydrophilic particles appeared darker than hydrophobic ones after treatment, indicating that hydrophilic particles adsorbed a higher amount of asphaltenes. This observation was verified with experiments using near-infrared spectroscopy that monitored the intensity of the stretching vibration of methylene groups (2924 cm^{-1}), which represented a convenient measure of the hydrocarbon content present on the silica surface. These results confirmed that the amount of asphaltenes adsorbed increased with an increase in the hydrophilicity of the particle surfaces. In a subsequent study, Dudášová and co-workers used UV−vis spectrometry to monitor the adsorption of asphaltenes on a variety of inorganic particles, including hydrophilic and hydrophobic SiO_2 (6). The asphaltene adsorption increased for the hydrophilic SiO_2 particles relative to the hydrophobic ones.

In spite of offering important insight into the effect of the amphiphilicity of the substrate on asphaltene adsorption, these studies were limited to only a few discrete surface types. In order to firmly ascertain the role of hydrophobicity on asphaltene adsorption, one needs to vary the surface energy of the substrate methodically. In previous work (18), we altered systematically the surface energy of the substrate by depositing self-assembled monolayers (SAMs) with smoothly varying chemical composition (25) and studied the effect of the substrate wettability, aromaticity, and organic layer thickness on asphaltene adsorption. We concluded that, although the chemistry of the substrates was carefully controlled, the wettability of the substrate was not the leading factor controlling the extent of asphaltene adsorption. Instead, we found that the extent of adsorption was controlled by the thickness of the underlying SAM, suggesting that the interaction between asphaltenes and the underlying polar silicon substrate was the most important factor governing the asphaltene adsorption process. In this paper, we build upon our previous findings and study asphaltene adsorption on aliphatic SAM surfaces by systematically increasing the length of the aliphatic spacer (or, equivalently, the number of carbon atoms, N_C, in the hydrocarbon mesogen). A clear picture of the physical and chemical property changes induced by chemical modification and asphaltene adsorption onto these substrates can potentially aid in the design of robust, asphaltene-repellent coatings for the inner walls of the oil pipelines.

The wettability, thickness, and carbon density of the hydrophobic SAMs are characterized by means of CA measurements, variable-angle spectroscopic ellipsometry (VASE), and near-edge X-ray absorption fine structure (NEXAFS) spectroscopy. The extent of asphaltene adsorption on these SAM surfaces is assessed using NEXAFS and VASE. Our primary aim is to verify that increasing the length of the SAM molecules and keeping the chemical nature of the SAM surfaces unchanged results in a decreased amount of ad-

sorbed asphaltenes on such SAM surfaces. Additionally, we will report on the effect of the solvent quality on the thickness of the adsorbed asphaltene layer. We will provide evidence that the extent of asphaltene adsorption increases with a decrease in the solubility of the asphaltenes in the solvent. Finally, we will reveal the importance of a thorough, multifaceted approach to characterizing the SAMs prior to their use in adsorption experiments, as evidenced by the effect of variation of the SAM properties on the extent of adsorption of asphaltenes on the surface.

MATERIALS AND METHODS

Materials. n-Butyl- (BTS), n-hexyl- (HTS), n-octyl- (OTS), n-decyl- (DTS), n-dodecyl- (DDTS), n-hexadecyl- (HDTS), and n-octadecyl- (ODTS) trichlorosilanes were purchased from Gelest, Inc. (Morrisville, PA), and used as received. HPLC-grade n-heptane and toluene were received from Fisher Scientific, 1,2,3,4-tetrahydronaphthalene (tetralin) and 1-methylnaphthalene (1-MN) were obtained from Sigma-Aldrich, and absolute ethanol was supplied by Acros Organics. All solvents were used as received. Silicon wafers (orientation [100]) were supplied by Silicon Valley Microelectronics (Santa Clara, CA). Hondo (HOW) crude oil for asphaltene precipitation was donated by Exxon-Mobil Upstream Research Company (Houston, TX). Hondo crudes had 14.8 % (w/w) asphaltene content with a hydrogen-to-carbon ratio of 1.29. The asphaltene precipitation was described elsewhere (26). Briefly, asphaltenes were obtained by mixing n-heptane and crude oil in a 40:1 weight ratio followed by stirring for 24 h. The mixture was subsequently filtered, and the asphaltenes were sequentially Soxhlet-extracted with n-heptane and toluene for 24 h each. The toluene was evaporated, and the asphaltenes were redissolved in methylene chloride for transfer. The asphaltenes were finally dried under reduced pressure, resulting in a shiny, dark solid.

Sample Preparation. Silicon wafers were cut into small (1 × 2 cm^2) pieces and cleaned by rinsing with absolute ethanol and exposure to an ultraviolet/ozone (UVO) treatment for 15 min. The latter process generated a high density of surface-bound −OH groups needed for SAM attachment. Deposition solutions of organosilanes were prepared inside a glovebag purged with nitrogen. A known amount of alkyltrichlorosilane was dissolved into HPLC-grade toluene to make stock solutions of high concentration (≈1 % trichlorosilane by weight). These stock solutions were diluted to a final concentration of 2 mmol of trichlorosilane/1 kg of solution. Trichlorosilane SAMs were deposited by submerging UVO-treated silicon substrates into deposition solutions in tightly sealed containers for ≈16 h. After SAM formation, the substrates were removed from the deposition solutions, quickly rinsed with toluene, and blow-dried with nitrogen gas. Several replicas of each sample were made in order to establish the properties of the pre- and post-asphaltene-treated SAMs and generate a sufficient level of confidence in our adsorption experiments.

Asphaltene solutions (0.5 % w/w) were prepared by dissolving the precipitated, dry asphaltenes in the respective solvent, followed by overnight shaking. Prior to use, the solutions were filtered in order to remove any undissolved solids. The asphaltene treatment was accomplished by exposing the SAM-covered substrates to these solutions for ≈12 h. The samples were subsequently rinsed and sonicated in a respective pure solvent for 5 min in order to remove any weakly adsorbed asphaltenes or remaining precipitated particles. After sonication, the samples were rinsed with toluene and blow-dried with nitrogen gas.

Spectroscopic Ellipsometry. The thicknesses of bare SAMs and SAM−asphaltene layers were determined with a variable-angle spectroscopic ellipsometer (J. A. Woollam Co., Lincoln, NE). Ellipsometry measures the difference in the polarization state between the light beams incident and reflected from the surface; it provides information about the thickness and dielectric properties of the film. Unless otherwise specified, ellipsometric data were collected at an incidence angle of 75° and at wavelengths ranging from 400 to 1100 nm in 20 nm increments. The ellipsometric angles Ψ and Δ depend on the thickness and dielectric constant of the probed film. While in most cases one can determine the optical constants and thicknesses from the ellipsometric data, for very thin films, these parameters are highly correlated and cannot be decoupled readily (27, 28). In order to estimate the thickness of the SAMs, we assumed the value of the index of refraction ($n = 1.50$) (29) and kept it constant throughout the fitting procedure. We note that variation of the refractive index of the film by ±0.05 results in an uncertainty of approximately ±1 Å (30). Even though we cannot determine the exact thickness of the film with complete certainty, the estimated thickness is important for comparison between different samples and previously published results.

CA Measurements. CAs (θ) with deionized (DI) water as the probing liquid were measured with a Ramé-Hart CA goniometer (model 100-00). Static CAs were determined after release of an 8 μL droplet of DI water on the surface. To measure the advancing and receding CAs (A-CA and R-CA, respectively), we captured the droplet with the syringe and added (advancing) or removed (receding) DI water from the droplet until the three-phase contact line was displaced. This procedure was repeated for three different spots on each sample, and the results were averaged. The A-CAs provide an estimate of the wettability of the SAMs. A densely packed SAM of aliphatic chains should form a very hydrophobic surface, which exhibits a high water CA ($\theta \approx 110°$). In addition, the CA hysteresis (CAH), defined here as the difference between A-CA and R-CA, provides information about the chemical and structural heterogeneities of the SAM. CAH of <10° is generally considered a signature of a largely uniform surface (23).

NEXAFS Spectroscopy. NEXAFS data were collected at the NIST/Dow Materials Characterization Facility (beamline U7A) of the National Synchrotron Light Source at Brookhaven National Laboratory (Upton, NY). NEXAFS involves the excitation of core-shell electrons by a monochromatic beam of soft X-rays and a subsequent relaxation process involving the emission of Auger electrons and fluorescence radiation. NEXAFS can discriminate between different chemical elements by tuning the energy of the incoming synchrotron X-ray beam to match the energy of the elemental core-shell electrons. Furthermore, resonances of specific electronic transitions from the core shell to unoccupied antibonding orbitals endow NEXAFS with sensitivity to the chemical environment of the film. The angle between the electric field vector of the X-ray beam and the sample normal was set to 55°; in this geometry, the NEXAFS signal is approximately independent of the average molecular orientation in the film (31). The X-ray absorption events were monitored with partial electron yield (PEY) and fluorescence yield (FY) detectors. The PEY detector was operated at a −150 V bias in order to detect only those electrons that originated from the topmost ≈2 nm of the sample (32). The FY detection mode is complementary to PEY in that it increases the probing depth of NEXAFS to hundreds of nanometers (31). Monitoring both the PEY and FY provides information about the surface and bulk compositions, respectively, of the films. One has to bear in mind that the signal-to-noise ratio depends crucially on the thickness of the probed film. In Figure 1, we plot PEY (top) and FY (bottom) NEXAFS spectra for SAMs of trichlorosilanes of varying chain length. Although the FY signal allows for characterization of the "bulklike" structure of the films, the signal-to-noise ratio is substantially decreased compared to PEY. Longer counting times are needed (5−10 times relative to PEY) in order to collect statistically meaningful spectra. The NEXAFS edge jump is defined as the difference between the postedge region (arbi-
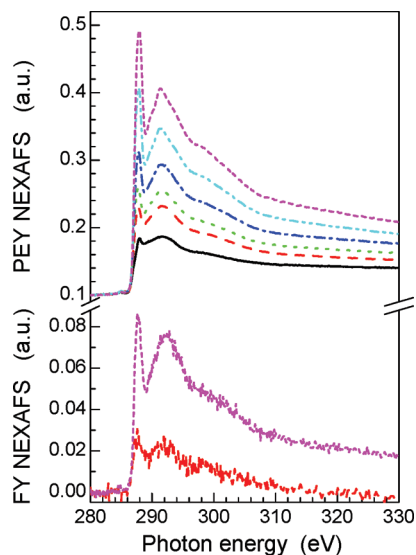
ACS **APPLIED** MATERIALS & INTERFACES

1349

FIGURE 1. PEY (top) and FY (bottom) NEXAFS spectra at the "magic" angle of incidence ($\theta = 55°$, where θ denotes the angle between the surface normal and the electric vector of the X-ray beam) for alkyltrichlorosilanes of varying chain length: *n*-butyltrichlorosilane (black —), *n*-octyltrichlorosilane (red − −), *n*-decyltrichlorosilane (green · · ·), *n*-dodecyltrichlorosilane (blue − · −), *n*-hexadecyltrichlorosilane (light blue − · · −), *n*-octadecyltrichlorosilane (pink ---). The preedge region of all of the PEY spectra (around 280 eV) has been shifted up by 0.1 au vertically for clarity.

trarily chosen at ≈320 eV) and the preedge region (arbitrarily chosen at ≈280 eV) of the spectrum. Depending on the detection method and the thickness of the probed film, the edge jump offers a convenient measure of the total amount of carbon probed in the film. In our experiments, the NEXAFS edge jump was monitored for at least three independent spots on each sample in order to ensure reproducibility of the data reported.

RESULTS AND DISCUSSION

SAMs represent an important tool for engineering surfaces through the modification of their physicochemical properties (23). Since their introduction in the 1980s by Sagiv and co-workers (33−39), organosilanes on silica have been one of the most widely used methods for the production of well-organized SAMs because of their thermal and chemical stability. The stability of organosilane SAMs results from covalent bonding of organosilanes to the substrate as well as an in-plane polysiloxane network formed among neighboring molecules in the vicinity of the substrate (33, 40, 41). This network endows organosilane-based SAMs with much higher stability relative to other SAMs, for example, those formed by assembling thiol-based moieties on noble metal surfaces. Wasserman et al. (42) employed ellipsometry, CA, XPS, and X-ray reflectivity to characterize the structure, stability, and reactivity of SAMs of *n*-alkyltrichlorosilanes of varying chain length. The authors reported that the SAMs formed possessed very high packing density for chain lengths larger than four carbon atoms; their data support a model of chains with an all-trans configuration oriented nearly parallel to the surface normal.

We prepared SAMs made of BTS, HTS, OTS, DTS, DDTS, HDTS, and ODTS using the protocols outlined in the Materials and Methods section. The bare SAMs were characterized thoroughly prior to the deposition of asphaltenes to inves-
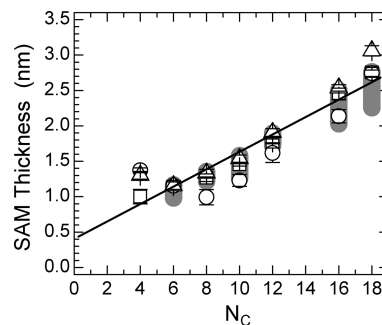

FIGURE 2. Thicknesses of the SAM measured by ellipsometry as a function of N_C for experiments collected at different times: November 2007 (□), March 2008 (○), and April 2008 (△). The gray bars represent the ranges of thicknesses reported by Wasserman et al. (42). The dotted line represents the best linear fit through the data.

tigate the effects of the thickness, wettability, and carbon content of the films on the extent of asphaltene adsorption. The ellipsometric thickness of the SAMs as a function of the number of carbon atoms in the alkyl mesogen of the organosilane chain (N_C) is plotted in Figure 2. The different symbols in Figure 2 denote samples prepared and characterized at different times. The thicknesses of the SAMs are reproducible from experiment to experiment and are consistent with the results reported previously in the literature. The gray bars behind the data in Figure 2 represent the range of SAM thicknesses reported by Wasserman et al. (42). The close agreement between our data and the results reported by Wasserman et al. is remarkable given that organosilane SAMs are well-known for their lack of reproducibility between different laboratory facilities and preparation protocols. We should mention that the thicknesses reported by Wasserman et al. were obtained by assuming that the refractive index of the film was 1.45, which is different from the one assumed here. As mentioned earlier, this assumption introduces thickness uncertainties in the Angstrom regime; these results are thus consistent despite the difference in the refractive index. The ellipsometric results support a model of alkyl chains in an all-trans configuration and oriented parallel to the surface normal. A best linear fit of the data yields the equation

$$t(N_C) = 1.23N_C + 4.09 \qquad (1)$$

where $t(N_C)$ is the thickness of the SAM in angstroms and N_C is the number of carbon atoms in the alkyltrichlorosilane chain. The thickness of the SAM increases by 1.23 Å per carbon atom in the organosilane molecule, a value that closely resembles that obtained by Wasserman et al. Extrapolation of the data to $N_C = 0$ results in an intercept of ≈4.09 Å; this value is consistent with the size of the head group in the SAM-forming molecules. In addition to the head group, a small amount of adventitious impurities might also contribute to the positive value of the intercept in eq 1.

In order to determine the carbon content of the SAMs, we extract the edge jump from the NEXAFS spectra and monitor its variation with the chain length (cf. Figure 3). The
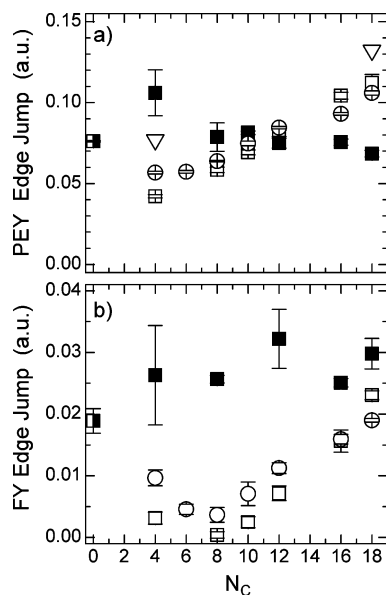
FIGURE 3. PEY (a) and FY (b) NEXAFS edge jump as a function of N_C for bare SAMs (open symbols) and asphaltene-treated SAMs (closed symbols). The data presented have been collected during various time periods: March 2007 (triangles), November 2007 (squares), and March 2008 (circles). The PEY and FY signals corresponding to bare silica treated with asphaltenes are shown for comparison (a half-filled symbol at $N_C = 0$).

proper interpretation of the edge jump requires consideration of the probing depth of the detection method (PEY vs FY) and the thickness of the probed material. Figure 3 depicts the (a) PEY and (b) FY NEXAFS edge jumps as a function of N_C for the alkyltrichlorosilane SAMs (open symbols). The PEY edge jump increases steadily with increasing N_C because of the increased amount of carbon present in the SAM. Extrapolation of the PEY edge jump data to $N_C = 0$ yields a value of the edge jump of ≈0.03 in the arbitrary unit scale. In contrast to the ellipsometry data, we cannot attribute this to the size of the head group in the organosilane molecule because NEXAFS data collected at the carbon K-edge is only sensitive to carbon atoms at the photon energies used. There are several factors that may contribute to the positive value of the intercept. First, there may be small amounts of adventitious carbon adsorbed on the surface. Second, we recall that the probing depth of the PEY NEXAFS technique is ≈2 nm (32) and that the thickness of SAMs with $N_C > 12$ is higher than the probing depth. This will result in lower than expected edge jumps for the long alkyl chains. Finally, the SAMs with $N_C < 8$ have a propensity to form multilayers, resulting in higher edge jump values. The combined effects of these three factors may explain the positive intercept of the edge jump trend. We provide a detailed account of the PEY data in relation to the SAM thickness in the Appendix. Similar to the PEY, the FY data increase with an increase in N_C. In the FY case, however, the extrapolated value at $N_C = 0$ yields a negative intercept; moreover, there are strong deviations from the aforementioned trend for $N_C < 8$. We attribute the FY trends to the inability of the FY detector to collect sufficient signals from very short SAMs. Thus, because of technical limitations, a certain minimum amount of carbon atoms needs to be
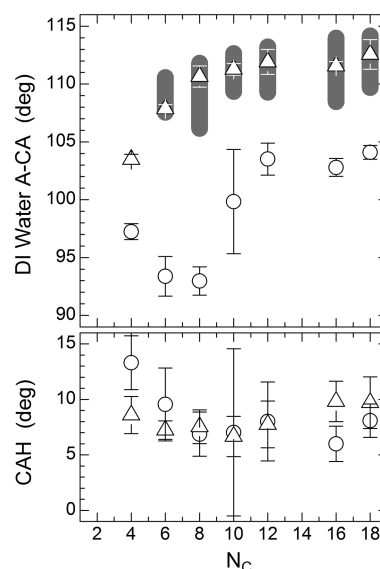

FIGURE 4. A-CA (top) and CAH (bottom) as a function of N_C shown for the March 2008 (○) and April 2008 (△) experiments. The gray bars represent the range of CAs reported by Wasserman et al. (42).

probed to detect a meaningful FY signal. It appears that, for the setup used, this minimal signal threshold would correspond to $N_C \approx 8$. The data in Figure 3 additionally include experiments performed at different dates, revealing the scatter induced by changes in the state of the detectors as well as demonstrating the high level of reproducibility of this measurement.

In Figure 4, we plot the advancing CAs (A-CAs) and the CAH as a function of N_C. The A-CAs exhibit two different trends for two distinct sets of samples prepared. The samples prepared in March 2008 (open circles) exhibit increasing values of the A-CA with an increase in N_C, ranging from ≈93° to a maximum of ≈104°. This set of samples also exhibits a sharp increase in the A-CA upon an increase in N_C from 8 to 10. The samples prepared in April 2008 (open triangles) exhibit a constant A-CA as a function of the alkyl chain length, except in the regime of very short chains, where a decrease in the A-CA is detected. The April 2008 data are in close agreement with literature values, as can be seen by the range of values extracted from Wasserman et al.'s work (gray bars in Figure 4). These two trends in the CA data suggest that the samples made in March 2008 did not pack as densely as expected. Despite the lower packing density of the March 2008 sample set, these experiments provide insight into the importance of surface wettability on asphaltene adsorption, as will be discussed below. The CAH does not exhibit a strong dependence on the alkyl chain length; it also does not exhibit the anomalous behavior seen in the A-CA data. This observation suggests that, although the March 2008 samples have lower packing densities and are therefore less hydrophobic, they possess a degree of chemical and structural homogeneity similar to that of the other data sets.

While the ellipsometry and NEXAFS edge jump data suggest that all of the SAMs studied here exhibit similar physical properties, the CA data show significant variation

for one of the experimental trials. Although the March 2008 samples exhibit consistent thicknesses and carbon content according to ellipsometry and NEXAFS, their A-CAs reveal clear deviations from the expected values. Proceeding with the asphaltene adsorption experiments without wettability data would have suggested that all SAMs were of equivalent quality and would have caused problems in the interpretation of the data. Therefore, we highlight the importance of characterizing engineered SAM surfaces with a wide range of experimental techniques because they often complement one another and no single technique can offer the full description of the system studied.

The extent of asphaltene adsorption can be studied by monitoring the variations in the edge jump before and after asphaltene treatment (cf. Figure 3). Because the adsorption of asphaltenes onto the SAMs results in an increase in the carbon content of the surface, it should be accompanied by an increase in the measured NEXAFS edge jump. The PEY edge jump NEXAFS data (cf. Figure 3a) reveal that with SAMs formed from alkyltrichlorosilanes with $N_C \leq 12$ the edge jump increases upon asphaltene adsorption. Conversely, SAMs with $N_C > 12$ exhibit a *decrease* in the edge jump. This deviation from the expected trends in the PEY data can be explained by considering the total thickness of the organic films upon asphaltene adsorption, the carbon density of the SAMs relative to the carbon density of passively adsorbed asphaltene films, and the probing depth of PEY NEXAFS. As discussed above, the thickness of the short-alkyl-chain SAMs is below the probing depth of PEY NEXAFS, which has been estimated by Sohn et al. to be ≈ 2 nm (32). Hence, these SAMs yield a small edge jump signal. When asphaltenes are adsorbed on short-alkyl-chain SAMs, the thickness of the overall organic film increases and the total amount of carbon probed increases, resulting in a net increase in the edge jump. However, for the long-alkyl-chain SAMs ($N_C > 12$), there is a net decrease in the PEY edge jump upon asphaltene adsorption. This decrease, although counterintuitive, is explained by recalling that the thickness of long-chain-length SAMs likely exceeds the probing depth of PEY NEXAFS. Auger electrons originating from long-alkyl-chain SAMs lose some energy while going through the asphaltene layer, resulting in electrons that cannot reach the PEY detector and therefore attenuation of the PEY NEXAFS signal (for a detailed discussion, see the Appendix). Additionally, if one assumes that the SAMs and the adsorbed asphaltene layer have equal carbon densities, one would expect the PEY NEXAFS edge jump signal to either remain constant or increase as the asphaltenes adsorb. Instead, we detect that the PEY NEXAFS edge jump signal decreases, indicating that the carbon density of the asphaltene layer is likely to be lower than that of the densely packed SAMs.
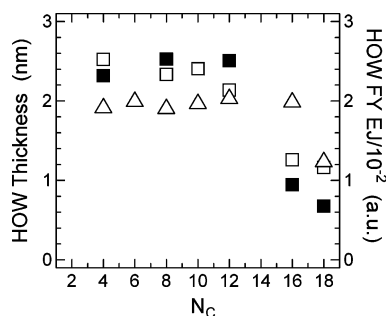
It is not surprising that the layer of passively adsorbed asphaltenes has a lower carbon atomic density than the SAMs. It is well-known that asphaltenes self-assemble in solution on form supramolecular aggregates that subsequently adsorb to the exposed surfaces. These bulk aggregates are known to entrain as much as 50 % (v/v) solvent

in the case of toluene (20, 43). Upon exposure of the asphaltene layer to a N_2 stream and to the high vacuum of the NEXAFS experiments, the solvent is removed from the asphaltenic aggregates. The presence of fused ring aromatic moieties in asphaltenic molecules, and their mutual orientation and juxtaposition in neighboring molecules, likely prevents the films from completely collapsing upon solvent removal. As a consequence, the asphaltenic molecules form a layer with significantly lower carbon atomic density relative to that of the well-packed hydrophobic aliphatic SAMs. Although this important information was obtained by means of the PEY NEXAFS measurements, the relatively shallow probing depth and difficulties associated with interpreting the amount of adsorbed asphaltenes with the PEY NEXAFS method highlight the need for complementary FY NEXAFS data to determine unambiguously the net amount of adsorbed asphaltenes.

In Figure 3b, we plot the FY NEXAFS edge jump before (open symbols) and after (solid symbols) asphaltene adsorption. With FY NEXAFS detection, the adsorption of asphaltenes always results in an increase in the edge jump signal, albeit a modest one for HDTS and ODTS SAMs. This is due to the large probing depth of the FY detection mode. The data in Figure 3b demonstrate that the FY NEXAFS edge jump of the bare SAMs increases with an increase in N_C. By contrast, the magnitude of the FY edge jump for asphaltene-treated SAMs remains approximately constant. These trends provide direct evidence that the amount of adsorbed asphaltenes on the SAM surfaces decreases with an increase in N_C, as will be discussed in detail later in this paper.

In order to further explicate the NEXAFS data, in Figure 3 we plot the PEY and FY NEXAFS edge-jump signals collected from a sample comprising an asphaltene layer adsorbed directly onto the silica substrate (half-filled square). The thickness of the resulting asphaltene layer is larger than the probing depth of PEY NEXAFS, as assessed by ellipsometry. The magnitude of the PEY NEXAFS edge jump collected from the asphaltene–SiO$_x$ sample is very close to the edge jumps of the asphaltene-treated SAMs but lower than the edge jumps of the thickest SAMs. This observation supports our earlier claim that the density of the asphaltene layer is lower than that of a well-organized SAM and that the decreases in the edge jump upon asphaltene adsorption are likely due to attenuation of the SAM signal. The FY NEXAFS edge-jump signal from a bare asphaltene-treated silicon wafer is also close to the signal of the asphaltene-treated SAMs, albeit slightly lower. While the asphaltene film is completely probed with FY NEXAFS, there is no contribution from the absent SAM, resulting in a slightly lower edge jump.
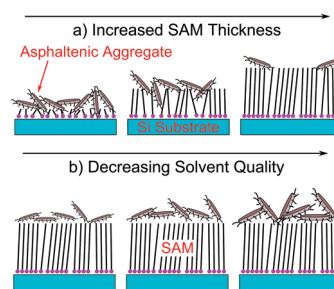
In order to verify the extent of asphaltene adsorption, we performed ellipsometry measurements on the asphaltene-treated SAMs. A three-layer model was employed in estimating the increase in the thickness due to asphaltene adsorption. The first and second layers represent the native silicon oxide and the SAM, respectively. The SAM layer is modeled as described before; its thickness is fixed to that for the bare SAMs shown in Figure 2. The third layer represents the

FIGURE 5. Thickness (open symbols, left ordinate) and the FY NEXAFS edge jump of asphaltene layers (closed symbols, right ordinate) adsorbed from toluene solutions and as a function of N_C in the underlying SAM. While the asphaltene layer thicknesses were measured directly by ellipsometry, the FY NEXAFS data were obtained by subtracting FY NEXAFS values collected from bare SAMs from those of the SAM−asphaltene specimens. The various symbols correspond to data collected in November 2007 (□ and ■) and April 2008 (△).

FIGURE 6. Schematics of asphaltenes adsorbed on alkyltrichlorosilane-modified silica substrates: (a) variations in adsorption with increased SAM thicknesses; (b) variations in the thicknesses of adsorbed asphaltenes with decreased solvent quality.

asphaltene layer; this layer is modeled by a uniform slab of constant index of refraction, n_{asph}, set to 1.8, a value obtained from ellipsometry measurements of spin-coated asphaltene from toluene solutions on clean silicon substrates (18). Because of the large thickness of the spin-coated asphaltene layer, the optical constants and thicknesses can be determined simultaneously and independently from the ellipsometry measurements. We note that $n_{asph} = 1.8$ is larger than the value normally estimated for asphaltenes in solution. Given that fused polyaromatic moieties can have refractive indices as high as ≈2.2 (44) and that asphaltenes comprise approximately 60 % aromatic hydrocarbons (21), one can estimate using an effective medium approximation (45) that the refractive index of asphaltenes should be ≈1.9. Although this estimated value is higher than the one measured by ellipsometry in this work, the apparent discrepancy can be explained by the inclusion of free volume in the asphaltenic aggregates, which are generated upon evaporation of an entrained solvent as explained above. We note that n_{asph} measured in an asphaltene spin-coated onto silica may differ slightly from that present in SAM-based layers because the packing density and chemical fractionation in these two sets of samples may not necessarily be equivalent. Nevertheless, given this approximation, assuming that $n_{asph} = 1.8$ provides a convenient means of estimating and comparing the asphaltene layer thickness from sample to sample.

The thickness of the asphaltene layer adsorbed from toluene solutions as a function of N_C is shown for two independent sets of experiments in Figure 5 (open symbols). The extent of asphaltene adsorption is nearly constant in the range of $3 < N_C < 16$. Upon an increase in N_C, the adsorbed amount of asphaltenes decreases sharply relative to the shorter SAMs. This result supports previous work on similar systems (18), in which the adsorption of asphaltene was found to decrease with an increase in thicknesses of the SAMs, an effect that was attributed to the decrease of the interaction between asphaltenes and the underlying silica substrate, as depicted schematically in Figure 6a. The data in Figure 5 also reveal the contribution of the adsorbed

asphaltenes on the SAMs of varying N_C to the FY NEXAFS edge jump signal of these samples. The results are consistent with ellipsometric data on the same samples (open squares) and confirm clearly a decrease in the adsorption of asphaltenes with an increase in the thickness of the SAM and the ability of FY NEXAFS to probe the entire thickness of the SAM−asphaltene films.

In addition to determining the dependence of the extent of asphaltene adsorption on N_C in the alkyltrichlorosilane SAMs, we established that the hydrophobicity of the SAM layer is of great importance in preventing the adsorption of asphaltenes and enhancing the reproducibility of the results. In Figure 4, we showed that SAMs with similar carbon content could exhibit different A-CAs, indicating that some experiments produced SAMs of lower hydrophobicity. We attributed this behavior to lower grafting densities of the SAM molecules, σ_{SAM}, on the substrate. In Figure 7, we plot the asphaltene thickness as determined with ellipsometry as a function of the negative cosine of the A-CA of the bare SAMs, $-\cos(\theta_{SAM})$ (46). Note that, because $\cos(\theta_{SAM})$ is proportional to the surface energy of the SAM substrate, it provides a measure of the cumulative effect of the SAM thickness (or, equivalently, N_C) and σ_{SAM}. From the data in Figure 7, the extent of asphaltene adsorption tends, for the most part, to decrease with an increase in the A-CAs. The higher wettabilities (i.e., lower A-CAs) are attributed to SAM layers that did not pack as densely as expected, possibly exposing methylene groups and/or the underlying polar silica to the asphaltene solution. This leads to a less obstructed interaction between the asphaltenes and the silica substrate. We therefore conclude that it is the coverage of the substrate by the SAMs, defined as a product of N_C and σ_{SAM}, that governs the effectiveness of the alkane "buffer" layer in minimizing the number of asphaltene−silica contacts.

Previous work established that a transition from liquidlike to semicrystalline-like structure of alkane-based SAMs occurs at N_C between 11 and 12 (25, 47−49). While we have not measured the conformation of the organosilanes in our SAM layers in this work directly, looking back at the data shown in Figure 4, it is tempting to attribute the sharp decrease in HOW at $N_C = 12$ to the formation of more-ordered semicrystalline SAMs, which would be more efficient in shielding the underlying silica substrate. Quantification of this conformational transition and its effect on adsorption will be the focus of future work.
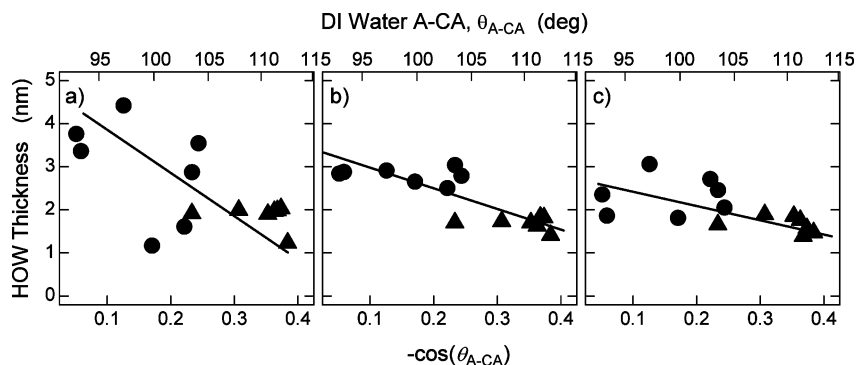
ACS APPLIED MATERIALS & INTERFACES

FIGURE 7. Thickness of the asphaltene-adsorbed film as a function of the negative cosine of the SAM DI water A-CA collected in the March 2008 (●) and April 2008 (▲) experiments shown for various solvents, including (a) toluene, (b) tetralin, and (c) 1-methylnaphthalene.

In addition to affinity to the SiO_x substrate, the extent of adsorption of any solute from the liquid phase depends on the substrate–solvent and solvent–solute interactions. So far, we have discussed adsorption of asphaltenes from toluene solutions and addressed the effect of modification of the characteristics of the underlying substrate, which affected the extent of the asphaltene–substrate interactions. We note that, in our analysis involving SAMs with different densities and length, we have ignored possible effects arising from various substrate–solvent effects. We now briefly address the effect of the solvent quality on the extent of asphaltene adsorption on alkyl SAMs. In Figure 7, we plot the HOW thickness for asphaltene adsorption from toluene (a), tetralin (b), and 1-MN (c) after sonication onto a variety of SAMs of varying N_C and carbon densities. The extent of asphaltene adsorption for 1-MN and tetralin is similar to that of toluene, suggesting either that the initial adsorption from these solvents is similar or that all of these solvents are equally effective at removing asphaltenes from the surface during the sonication step.

In order to discriminate between the initial adsorption of asphaltenes from different solvents and the ability of these solvents to clean the surface during the sonication step, we measured the amount of adsorbed asphaltenes on ODTS substrates of equivalent packing density before and after sonication. The data in Figure 8a depict the thickness of the adsorbed asphaltenes before (closed symbols) and after (open symbols) the sonication step as a function of the Hildebrand solubility parameter (δ) of the solvent (50). The asphaltene adsorption increases in the following order: 1-MN < tetralin < toluene < decalin < Heptol [20:80 (w/w) *n*-heptane–toluene]. Note that the solubility parameter of the solvent increases in the same manner. The value of δ of asphaltenes has been estimated to range between 19.5 and 20.5 $MPa^{1/2}$ (51–53). From the data in Figure 8a, the thickness of the asphaltene layer both before and after sonication in the neat solvent decreases systematically with increasing δ. This trend is identical with the variation of the asphaltene aggregate size measured earlier by small-angle neutron scattering experiments (22) (cf. Figure 8b). Because asphaltenes are known to form oblate cylindrical supramolecular aggregates, it is tempting to conclude that roughly a monolayer of aggregates adsorbs onto these surfaces. The mean diameter of these discoidal aggregates (crossed sym-
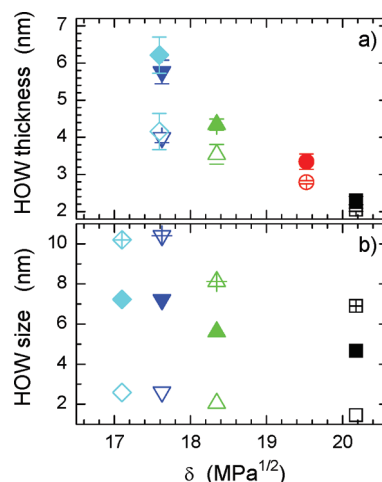

FIGURE 8. (a) Thickness of the asphaltene-adsorbed film before (closed symbols) and after (open symbols) sonication in parent neat solvent and (b) the aggregate size (aggregate diameter, crossed symbols; aggregate thickness, open symbols; aggregate average radius of gyration, closed symbols) as a function of the Hildenbrand solubility parameter of the solvent. The solvents used are Heptol (cyan ◇), decalin (blue ▽), toluene (green △), tetralin (red ○), and 1-MN (black □). The composition of Heptol in samples in Figure 8a is 20:80 (w/w), while that in samples in Figure 8b is 60:40 (v/v). The data in Figure 8b have been adopted from ref 22.

bols in Figure 8b) varies from 7 nm in 1-MN to slightly more than 10 nm in decalin and mixtures of heptane and toluene. The thicknesses of these aggregates (open symbols in Figure 8b) are 1.5–2.6 nm, depending on the solvent quality (20, 22, 43). The adsorbed asphaltene thickness in Figure 8a, before and after sonication, suggests that upon adsorption a wide distribution of orientations of these discoidal aggregates may exist on the surface, with some of the aggregates adsorbed face on and some adsorbed edge on. Sonication may remove the more weakly adsorbed aggregates. The difference between the aggregate diameter and thickness is greatest for the larger aggregates, those adsorbed from heptane–toluene mixtures and decalin, and it is smallest for the best solvent, 1-MN. This may explain the trend in Figure 8a, in which large amounts of asphaltenes are removed from the surface upon sonication in Heptol while a very small amount of asphaltenes are detached when the sonicating medium is 1-MN. These observations are schematically depicted in Figure 6b and indicate that, in addition to the physicochemical properties of the surface, the solution state of the asphaltenic aggregates plays an

important role in the ability of the asphaltenes to be adsorbed onto and cleaned from solid surfaces.
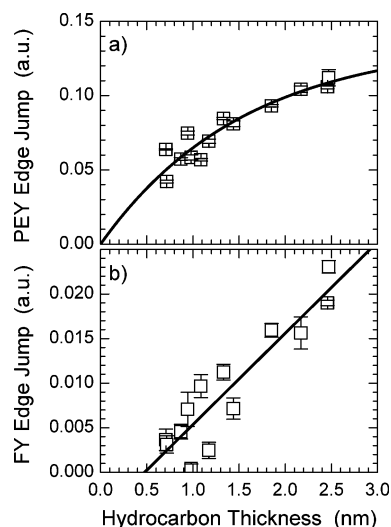
CONCLUSIONS

We have shown that chemical modification of model silicon substrates with organosilane SAMs results in coatings capable of minimizing asphaltene adsorption. Considering that organosilane coatings can generally be applied to a wide range of substrates, including oxide-coated materials used in petroleum pipelines, the findings reported here could aid in an effective design of coatings enabling protection of oil-transport pipelines against asphaltene adsorption and accumulation. CA measurements, spectroscopic ellipsometry, and NEXAFS spectroscopy have been employed to determine the extent of asphaltene adsorption onto model SAMs made of trichlorosilanes with varying chain lengths. Our measurements and analysis reveal that the most important factor governing the adsorption of asphaltenes onto the substrates is the ability of the SAM layer to shield the underlying silica substrate from interaction with the polar functional groups on the asphaltenic aggregates present in solution. This conclusion was reached by noting a decrease in asphaltene adsorption with an increase in the thickness of the SAM layers. Additionally, experiments performed on SAMs that exhibited lower than expected A-CAs revealed increased amounts of adsorbed asphaltenes. This observation was reconciled by considering the lower packing density of the SAM molecules likely in those surfaces with lower A-CAs, which, in turn, results in a higher exposure of the silicon substrate to the asphaltene solution. Adsorption experiments from different solvents revealed that asphaltene adsorption decreased with an increase in the solubility parameter of the deposition solvent for all solvents studied here. In the analysis of these adsorption experiments, we explored some of the considerations necessary when performing NEXAFS spectroscopy studies of thin films. Specifically, we compared PEY and FY NEXAFS detection modes and discussed their limitations and advantages. We demonstrated that careful consideration should be given to the thickness of the probed film, its atomic density as a function of the depth from the surface, and the probing depth of the detection mode used in NEXAFS.

APPENDIX: DETERMINATION OF THE ESCAPE DEPTH FOR PEY NEXAFS

The application of SAMs with systematically varying lengths of the alkyl mesogens in the trichlorosilanes enabled us to establish that a correlation exists between the NEXAFS edge jump

FIGURE 9. Edge jump of the trichlorosilane SAMs as a function of the adjusted SAM thickness for (a) PEY NEXAFS and (b) FY NEXAFS. The solid line in part a represents a best fit to eq A1. The solid line in part b is meant to guide the eye.

and the ellipsometric thickness of the SAMs (or, equivalently, N_C). While discussing the dependence of the NEXAFS edge jump on N_C, we briefly pointed out the advantages and disadvantages of both NEXAFS detection methods, the PEY and FY modes. A better understanding of the capabilities and shortcomings of each detection mode is acquired when we compare the NEXAFS edge jump to the thickness of the alkyl mesogen of the SAMs (cf. Figure 9). The adjusted thickness is obtained by subtraction of the thickness of the organosilane head group from the total SAM thickness. This is necessary because the NEXAFS edge jump at the carbon K-edge only probes the carbonaceous material on the surface, whereas ellipsometry measures the total thickness of the SAM, including both the silane head group and the carbon-containing alkyl chain. To accomplish this adjustment, we assume that the chains are in an all-trans conformation and subtract a value of 2.85 Å from the total SAM thickness, a number obtained by adding the z-axis projections of a carbon–silicon bond and a silicon–oxygen bond (42, 54). Note that, in addition to the carbon present in the SAMs, there is very likely some adventitious carbon contamination present on the sample. When is it assumed that, to the first approximation, the atomic density of adventitious hydrocarbon is similar to that present in the SAM, the correlation between the NEXAFS edge jump and the hydrocarbon thickness (HT) measured by ellipsometry is not affected by the adventitious carbon because the chemical compositions of the impurities are very likely similar to those of the SAM and will have comparable dielectric constants (affecting the ellipsometry measurements) and escape depths (affecting the NEXAFS measurements).

Figure 9a displays the PEY edge jump as a function of the HT. While the data in Figure 2 showed a nearly linear dependence of the PEY edge jump on N_C, the same cannot be said about the edge-jump dependence on the HT. A simple model of the observed Auger electron signal as a function of the thickness of the probed hydrocarbon layer can be constructed, as shown in Figure 10. We assume that the intensity of the Auger electrons originating from an infinitesimally thin slab of the probed material a distance z from the substrate is I_0. These electrons travel through a
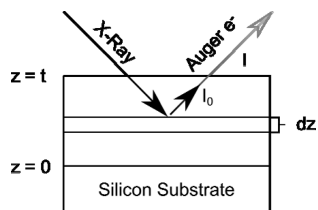
FIGURE 10. Schematic showing a simple model, from which eq A1 can be derived.

distance (HT − z) of carbonaceous material before escaping to the vacuum in the NEXAFS chamber and reaching the PEY detector. Given this model, we can write

$$I = \int_0^{HT} I_0 e^{-(HT-z)/\lambda}\, dz = I_0 \lambda (1 - e^{-HT/\lambda}) \qquad (A1)$$

where λ is the inelastic mean free path of the Auger electrons, whose intensity in the detector is I. A best fit to the data using eq A1 yields values of $\lambda = 1.55 \pm 0.32$ nm and $I_0 = 0.088 \pm 0.008$ au/nm. We note that the value of λ is close to that recently reported by Sohn et al. ($\lambda = 1.95$ nm) (32).

In Figure 9b, we plot the FY NEXAFS edge jump as a function of the HT. As mentioned in the main part of the paper, a plot of the FY edge jump versus N_C, extrapolated to HT = 0, yields a negative value of the FY edge jump. A plausible explanation for this is that a minimum amount of carbon probed has to be present on the surface in order to be detectable via FY NEXAFS. An equation like eq A1 can be written for fluorescent radiation, but the parameter λ is replaced by λ' and increases to hundreds of nanometers. The FY data obtained from SAMs are in the limit of small t/λ' and thus precludes us from determining λ'. A best linear fit to the FY data suggests that the minimum thickness of the carbonaceous material that we are able to detect is HT = 0.476 ± 0.205 nm. Additionally, for small t/λ', the slope of the best-fit line becomes $I_0 = 0.0102 \pm 0.0013$ au/nm. This is a measure of the intensity of fluorescent radiation emitted per 1 nm of material.

This discussion highlights the importance of carrying out NEXAFS measurements in both the PEY and FY detection methods. PEY NEXAFS should be used for probing of very thin (1−2 nm thickness) films; the actual thickness depends on the specific material studied. From the data in Figure 9, it is apparent that while the PEY signal for films thinner that λ exhibits a reasonably linear dependence on film thickness, upon reaching film thicknesses of around 3−4 multiples of λ, the signal levels off dramatically because not all Auger electrons can be successfully emitted from the sample and detected. In contrast, FY should be used for thicker films, for the case of hydrocarbons studied here; the minimal thickness is ≈0.5 nm. We expect that this minimal thickness is determined by the sensitivity of the given fluorescence detector and will likely remain the same for most soft materials. Overall, in order to characterize soft material films that span a large range of thickness, a dual-detection approach involving both PEY and FY measurements should be invoked when possible.

REFERENCES AND NOTES

(1) Leontaritis, K. J.; Ali Mansoori, G. *J. Pet. Sci. Eng.* **1988**, *1*, 229–239.

(2) Speight, J. G. *The Chemistry and Technology of Petroleum*; Chemical Industries, Marcel Dekker, Inc.: New York, 1999; Vol. 76, p 918.

(3) Drummond, C.; Israelachvili, J. *J. Pet. Sci. Eng.* **2004**, *45*, 61–81.

(4) Toulhoat, H.; Prayer, C.; Rouquet, G. *Colloids Surf. A* **1994**, *91*, 267–283.

(5) Akhlaq, M. S.; Götze, P.; Kessel, D.; Dornow, W. *Colloids Surf. A* **1997**, *126*, 25–32.

(6) Dudášová, D.; Simon, S.; Hemmingsen, P. V.; Sjöblom, J. *Colloids Surf. A* **2008**, *317*, 1–9.

(7) Batina, N.; Manzano-Martinez, J. C.; Andersen, S. I.; Lira-Galeana, C. *Energy Fuels* **2003**, *17*, 532–542.

(8) Batina, N.; Reyna-Cordova, A.; Trinidad-Reyes, Y.; Quintana-Garcia, M.; Buenrostro-Gonzalez, E.; Lira-Galeana, C.; Andersen, S. I. *Energy Fuels* **2005**, *19*, 2001–2005.

(9) Castillo, J.; Goncalves, S.; Fernández, A.; Mujica, V. *Opt. Commun.* **1998**, *145*, 69–75.

(10) Acevedo, S.; Castillo, J.; Fernandez, A.; Goncalves, S.; Ranaudo, M. A. *Energy Fuels* **1998**, *12*, 386–390.

(11) Acevedo, S.; Ranaudo, M. A.; Garcia, C.; Castillo, J.; Fernandez, A.; Caetano, M.; Goncalvez, S. *Colloids Surf. A* **2000**, *166*, 145–152.

(12) Acevedo, S.; Ranaudo, M. A.; Garcia, C.; Castillo, J.; Fernandez, A. *Energy Fuels* **2003**, *17*, 257–261.

(13) Ekholm, P.; Blomberg, E.; Claesson, P.; Auflem, I. H.; Sjöblom, J.; Kornfeldt, A. *J. Colloid Interface Sci.* **2002**, *247*, 342–350.

(14) Xie, K.; Karan, K. *Energy Fuels* **2005**, *19*, 1252–1260.

(15) Dudášová, D.; Silset, A.; Sjöblom, J. *J. Dispersion Sci. Technol* **2008**, *29*, 139–146.

(16) Abdallah, W. A.; Taylor, S. D. *Nucl. Instrum. Methods Phys. Res., Sect. B* **2007**, *258*, 213–217.

(17) Labrador, H.; Fernandez, Y.; Tovar, J.; Munoz, R.; Pereira, J. C. *Energy Fuels* **2007**, *21*, 1226–1230.

(18) Turgman-Cohen, S.; Smith, M. B.; Fischer, D. A.; Kilpatrick, P. K.; Genzer, J. *Langmuir* **2009**, doi:10.1021/la9000895.

(19) Alboudwarej, H.; Pole, D.; Svrcek, W. Y.; Yarranton, H. W. *Ind. Eng. Chem. Res.* **2005**, *44*, 5585–5592.

(20) Gawrys, K. L.; Kilpatrick, P. K. *J. Colloid Interface Sci.* **2005**, *288*, 325–334.

(21) Gawrys, K. L.; Blankenship, G. A.; Kilpatrick, P. K. *Energy Fuels* **2006**, *20*, 705–714.

(22) Verruto, V. J.; Kilpatrick, P. K. *Energy Fuels* **2007**, *21*, 1217–1225.

(23) Ulman, A. *An Introduction to Ultrathin Organic Films: from Langmuir−Blodgett to Self-assembly*; Academic Press: Boston, 1991; p 442.

(24) Hannisdal, A.; Ese, M.; Hemmingsen, P. V.; Sjöblom, J. *Colloids Surf. A* **2006**, *276*, 45–58.

(25) Smith, M. B.; Efimenko, K.; Fischer, D. A.; Lappi, S. E.; Kilpatrick, P. K.; Genzer, J. *Langmuir* **2007**, *23*, 673–683.

(26) Spiecker, P. M.; Gawrys, K. L.; Kilpatrick, P. K. *J. Colloid Interface Sci.* **2003**, *267*, 178–193.

(27) McCrackin, F. L; Passaglia, E.; Stromberg, R. R.; Steinberg, H. L. *J. Res. Natl. Bur. Stand., Sect. A* **1963**, *A 67*, 363–377.

(28) McCrackin, F. L.; Passaglia, E.; Stromberg, R. R.; Steinberg, H. L. *J. Res. Natl. Inst. Stand. Technol.* **2001**, *106*, 589–603.

(29) Wasserman, S. R.; Whitesides, G. M.; Tidswell, I. M.; Ocko, B. M.; Pershan, P. S.; Axe, J. D. *J. Am. Chem. Soc.* **1989**, *111*, 5852–5861.

(30) Tillman, N.; Ulman, A.; Schildkraut, J. S.; Penner, T. L. *J. Am. Chem. Soc.* **1988**, *110*, 6136–6144.

(31) Stöhr, J. *NEXAFS Spectroscopy*; Springer Series in Surface Sciences 25; Springer-Verlag: New York, 1992; p 403.

(32) Sohn, K. E.; Dimitriou, J.; Genzer, J.; Fischer, D. A.; Hawker, C. J.; Kramer, E. J. *Langmuir* **2009**, in press.

(33) Sagiv, J. *J. Am. Chem. Soc.* **1980**, *102*, 92–98.

(34) Netzer, L.; Sagiv, J. *J. Am. Chem. Soc.* **1983**, *105*, 674–676.

(35) Netzer, L.; Iscovici, R.; Sagiv, J. *Thin Solid Films* **1983**, *99*, 235–241.

(36) Netzer, L.; Iscovici, R.; Sagiv, J. *Thin Solid Films* **1983**, *100*, 67–76.

(37) Maoz, R.; Sagiv, J. *J. Colloid Interface Sci.* **1984**, *100*, 465–496.

(38) Gun, J.; Iscovici, R.; Sagiv, J. *J. Colloid Interface Sci.* **1984**, *101*, 201–213.

(39) Gun, J.; Sagiv, J. *J. Colloid Interface Sci.* **1986**, *112*, 457–472.

(40) Finklea, H. O.; Robinson, L. R.; Blackburn, A.; Richter, B.; Allara, D.; Bright, T. *Langmuir* **1986**, *2*, 239–244.

(41) Allara, D. L.; Parikh, A. N.; Rondelez, F. *Langmuir* **1995**, *11*, 2357–2360.

(42) Wasserman, S. R.; Tao, Y. T.; Whitesides, G. M. *Langmuir* **1989**, *5*, 1074–1087.

(43) Gawrys, K. L.; Blankenship, G. A.; Kilpatrick, P. K. *Langmuir* **2006**, *22*, 4487–4497.

(44) McCartney, J. T.; Ergun, S. *J. Opt. Soc. Am.* **1962**, *52*, 197–200.

(45) Tompkins, H. G.; McGahan, W. A. *Spectroscopic Ellipsometry and Reflectometry*; John Wiley & Sons, Inc.: New York, 1999; pp 125–126.

(46) Using $-\cos(\theta_{SAM})$ instead of θ_{SAM} is physically more meaningful because, based on Young's equation, $\cos(\theta_{SAM}) = (\gamma_{SAM} - \gamma_{SAM/L})/\gamma_L$, where γ_{SAM} is the surface energy of the SAM layer, $\gamma_{SAM/L}$ is the interfacial energy at the SAM–probing liquid interface, and γ_L is the surface energy of the probing liquid; $-\cos(\theta_{SAM})$ is thus directly proportional to the physicochemical character of the SAM substrate and follows the same trend (i.e., it either increases or decreases) as θ_{SAM}.

(47) Allara, D. L.; Parikh, A. N.; Judge, E. *J. Chem. Phys.* **1994**, *100*, 1761–1764.

(48) Chaudhury, M. K.; Owen, M. J. *J. Phys. Chem.* **1993**, *97*, 5722–5726.

(49) Snyder, R. G.; Strauss, H. L.; Elliger, C. A. *J. Phys. Chem.* **1982**, *86*, 5145–5150.

(50) Yaws, C. L. *Chemical properties handbook: physical, thermodynamic, environmental, transport, safety, and health related properties for organic and inorganic chemicals*; McGraw-Hill Handbooks; McGraw-Hill: New York, 1999; p 779.

(51) Hirschberg, A.; Dejong, L. N. J.; Schipper, B. A.; Meijer, J. G. *Soc. Pet. Eng. J.* **1984**, *24*, 283–293.

(52) Burke, N. E.; Hobbs, R. E.; Kashou, S. F. *J. Pet. Technol.* **1990**, *42*, 1440–1446.

(53) Mannistu, K. D.; Yarranton, H. W.; Masliyah, J. H. *Energy Fuels* **1997**, *11*, 615–622.

(54) Alternatively, the thickness adjustment can be accomplished by subtracting 2.34 Å, a mean diameter of the silicon atom, from the total SAM thickness. Using this assumption, the value of λ is 1.72 ± 0.37 nm and that of I_0 is 0.008 ± 0.001 au/nm.

AM900203U